Theor Chem Acc (2009) 124:385–394
DOI 10.1007/s00214-009-0628-7

REGULAR ARTICLE

First principles calculations on the origin of violet-blue and green light photoluminescence emission in $SrZrO_3$ and $SrTiO_3$ perovskites

Valéria M. Longo · Laécio S. Cavalcante · Maria G. S. Costa · Mário Lúcio Moreira · Alberthmeiry T. de Figueiredo · Juan Andrés · José A. Varela · Elson Longo

Received: 22 June 2009 / Accepted: 18 August 2009 / Published online: 3 September 2009

Abstract The photoluminescence (PL) emission from $SrZrO_3$ (SZ) and $SrTiO_3$ (ST) crystalline, quasi-crystalline, and quasi-amorphous samples, prepared by the polymeric precursor method, was examined by ab initio quantum mechanical calculations. It was used in the modeling the structural model consisting of one pyramidal TiO_5 or ZrO_5 unit piled upon the TiO_6 or ZrO_6, which are representative of disordered structures of quasi-crystalline structures such as ST and SZ. The structural crystallization process was monitored by X-ray diffraction. In quasi-crystalline powders, the photoluminescence (PL) in the visible region showed different peak positions and intensities in SZ and ST. The PL emission was linked to distinct distortions in perovskite lattices and the emission of two colors—violet-blue in SZ and green in ST—was also examined in the light of favorable structural and electronic conditions.

Keywords Ab initio calculations · Perosvskite · Photoluminescence

This article renders tribute to Professor Dr. Ricardo Ferreira.

V. M. Longo (✉) · M. G. S. Costa · A. T. de Figueiredo · J. A. Varela · E. Longo
LIEC, Instituto de Química, UNESP, Araraquara, SP 14801-970, Brazil
e-mail: valerialongo@liec.ufscar.br

L. S. Cavalcante · M. L. Moreira (✉)
LIEC, Departamento de Departamento de Química, UFSCar, São Carlos, SP 13565-905, Brazil
e-mail: mlucio@liec.ufscar.br

J. Andrés
Departamento de Química Física y Analítica, Universitat Jaume I, 12071 Castelló, Spain

1 Introduction

Perovskite-type oxides are a class of materials that have been investigated extensively since the 1940s due to their significance to fundamental research and their high potential for technological applications [1]. Materials that crystallize in perovskite-type oxide structures have the general formula of ABO_3 (where A = Ca, Sr, Pb or Ba and B = Ti or Zr) and are among the most important materials for a variety of applications, as well as some of the most versatile for chemical tuning of composition and structure. These materials display a plethora of physical and chemical properties of technological interest that depend on processing conditions, oxygen content, and order [1–6].

Strontium zirconate, $SrZrO_3$ (SZ), is particularly interesting because of its high-temperature electronic properties [7]. Large single crystals of SZ of great perfection can be grown for applications as laser hosts and substrate materials such as fuel cells, steam electrolysis, and hydrogen gas sensors [8–10]. These properties are obtained when this oxide is doped with acceptor ions that exhibit protonic conduction at high temperature [11].

At room temperature SZ has an orthorhombic phase, as revealed by structural studies performed in the 1950s and 1960s [12, 13]. More recent studies [14–16] at high temperatures have shown that SZ undergoes three structural phase transitions, as follows: first, orthorhombic (*Pbnm*) to orthorhombic (*Cmcm*) at 697 °C, then to tetragonal (*I4/mcm*) at 827 °C, and finally to cubic (*Pm3 m*) at 1,127 °C. The experimental energy gap of SZ ranges from 5.22 to 5.50 eV [17, 18].

$SrTiO_3$ (ST) has a simple cubic perovskite structure and is a semiconductor with an indirect band gap, which usually ranges from 3.2 to 3.4 eV [19, 20]. By modifying its structure, this material can be made to display a variety of

physical properties. For example, a small amount of electron doping by chemical substitution of oxygen vacancies makes the material conducting and even superconducting at low temperatures [21, 22].

Several reports in the literature describe the conditions required for PL emission in materials presenting a degree of order–disorder [23–25]. However, there is no general consensus in the literature about why and how radiative decay takes place in perovskite-like structures with a certain degree of disorder [26].

Some authors ascribe the PL to deviation from stoichiometry and others to the presence of impurities. From the general phenomenology and the seminal idea of Landau [27], the intrinsic molecular polarons in ionic solids have a crucial effect and can be considered a characteristic subject of current research. The idea of self-trapping originally introduced by Landau describes an excess electron being trapped within a potential self-created well in a crystal. The electron, together with the locally distorted lattice around it, can be considered a quasiparticle, which is known as a polaron. In this respect, Qiu et al. [28] studied the relaxation process of self-trapped polarons by a nonadiabatic molecular dynamic method. These authors point out that localized disorder due to lattice fluctuations can give rise to a tightly bound electronic state in ultraviolet-illuminated $SrTiO_3$ crystal. This bound state is actually a self-trapped polaron, in accordance with the experimentally observed large Stokes-shift. The formation of the self-trapped polaron is an ultrafast process. Among the several mechanisms for analyzing the origins of PL in perovskite-based materials, the recombination of self-trapped excitons (STE) [29, 30], holes (excitons) and charge transfer vibronic excitons (CTVEs) [31] are the basis of the current proposals to interpret the PL behavior. Vikhnin et al. [32, 33] introduced the concept of CTVE to explain an exciton structure in ABO_3-type materials. CTVEs are multi-site structures that are induced by charged impurities in ionic-covalent solids [32]. A pair consisting of an electron polaron and a hole polaron is associated with a defect-bound or STE such as Ti^{+3}–O^{-} state in the TiO_6 octahedron. For strontium titanate ($SrTiO_3$), Vikhnin and Kapphan [34] proposed that the "green" luminescence corresponds to the recombination of the electron and the hole in the vibronic charge-transfer exciton, which is accompanied by the emission of light. In this respect, also for $SrTiO_3$, Leonelli et al. [29] point out that the visible emission is intrinsic in origin, corresponding to the recombination of a STE. Eglitis et al. [35] combined time-resolved absorption and luminescence spectra with quantum mechanical calculations at a semi-empirical level to study polaron optical properties in $KNbO_3$ perovskite associated with radiative recombination of self-trapped electrons and hole polarons. Meng et al. [36] proposed a visible emission model for nanocrystalline $A_{1-x}A'_xTiO_3$ systems (A = Ba, Sr, A′ = Pb), in which the electrons in the valence bands absorb photons and get excited to some localized sensitizing centers correlated with surface states in the forbidden gap, but not directly to a conduction band, with the electron polarons with holes forming STEs. However, both CTVE and STE models for ABO_3 ferroelectric materials converge in that they associate the strong electron–lattice interaction and exciton relaxation as being responsible for the large Stokes shift observed [23].

Green light PL emission of ST [37] and the intense violet-blue light emission of SZ [38] have already been reported. The PL emission was attributed to localized levels above the valence band (VB) and below the conduction band (CB) [37, 38]. In this context, PL emission has proved to be a powerful tool for investigating the energy levels of materials, offering important information about the physical properties of materials at the molecular level, including shallow and deep level defects and gap-states [39]. However, the exact nature of the recombination of PL emission is still controversial. In this context, using a local density approximation, Lee et al. [40] recently reported that oxygen vacancies tend to cluster in linearly in ST. This linear vacancy cluster and the appearance of the in-gap states explain many experimental results, such as transport behaviors and photoluminescence of oxygen-deficient ST. These findings may provide a viable route to understand various physical behaviors, specifically transport properties, of perovskite oxide, which is inherently prone to oxygen nonstoichiometry. They also suggest that the properties of materials can be influenced significantly by vacancy clusters throughout regions like interfaces or grain boundaries, where nonstoichiometry is often enhanced. To elucidate the mechanism of the blue-light emission process, Onishi [41] made hybrid-DFT calculations for oxygen-deficient cluster models, concluding that oxygen deficiency is irrelevant to the process because of the strong chemical bond between titanium atoms. These findings contradict the experimental results reported by Kan et al. [42–44], who observed blue-light emission in both oxygen-deficient and electron-doped $SrTiO_3$. Thus, it is believed that other factors such as conducting electrons play an important role in the blue-light emission process. Zhan et al. results indicate that the annealed ZrO_2 samples exhibit broad, intense visible photoluminescence and the annealing temperature is indispensable for the luminescence of the obtained ZrO_2 particles. The emission colors of the ZrO_2 samples can be tuned from blue to nearly white to dark orange by varying the annealing temperature [45].

In this paper, we present a comparative study of an intense and broad PL band at room temperature in quasi-

amorphous and quasi-crystalline SZ and ST powders excited by the 350.7 nm line of a Kripton ion laser. The origin of the intense PL bands was investigated based on electronic structure calculations carried out within the framework of ab initio periodic quantum-mechanical techniques. The evolution of order–disorder in the network former, Zr in the case of SZ and Ti in that of ST, and the different colors of PL emission, are also discussed in the light of the complex cluster concept.

2 Experimental section

Ordered and disordered SZ and ST powders were prepared by the polymeric precursor method [46]. Experimental details have been described elsewhere [17, 47]. This technique is well known and used extensively for the design and synthesis of advanced functional and engineering materials, including powders, films, fibers, and monoliths of almost any shape, size, and chemical composition [48, 49].

The polymeric SZ resin was pyrolized at 350 °C for 2 h, and the ST at 300 °C for 2 h, both resulting in powders containing organic residues due to the method employed. The SZ powders were annealed at 400, 475, and 660 °C for 2 h while the ST powders were annealed at 400, 450, and 550 °C, both in an oxygen flow atmosphere.

The SZ and ST powders were structurally characterized by X-ray diffraction (XRD) (with Cu K_α radiation). The diffraction patterns were recorded in a Bragg–Brentano diffractometer at Cu K_α in a $\theta - 2\theta$ configuration, using a graphite monochromator. For a better understanding of this work, it should be noted that two kinds of powders were involved: the first, structurally disordered, was heat-treated below the crystallization temperature, while the second one, structurally ordered, was crystallized. The PL spectra were collected with a Thermal Jarrel-Ash Monospec 27 monochromator and a Hamamatsu R446 photomultiplier. The 350.7 nm exciting wavelength of a krypton ion laser (Coherent Innova) was used, with the nominal output power of the laser kept at 200 mW.

3 Crystal structure

Knowledge of material structures at the atomic level is one of the workhorses of modern structural chemistry. This knowledge is the fist step toward an understanding of the behavior of materials, and the difficulty of accessing such structures is a major factor that limits our ability to fully investigate the chemistry and physics of systems and hinders our access to potentially useful materials.

Real solid materials are incredibly complex. They have an intricate band structure of allowed energy states, and the Coulomb interactions of electrons are difficult to account for. Disorder and the inevitable effects of vibrations of the crystal lattice add to this intricacy. It is not desirable, and usually impossible, to take all these effects into account simultaneously.

These problems can be circumvented partly by using computer simulations and theoretical calculations. Since most materials exhibit quantum phenomena, it is necessary to understand them from an atomistic point of view. On the computational side, theorists have been fine-tuning first-principle (ab initio) calculations so they can better understand the different properties. Without question, molecular simulations play a crucial role in facilitating the interpretation of experimental data at the atomic level.

Oxide perovskites are commonly described by the chemical formula ABO_3, where A represents cations with a large radius, B stands for cations with a small radius, and O denotes oxygens. The characteristic constituents of polyhedra are the octahedron and dodecahedron, i.e., the coordination number A is 12 (cube-octahedral polyhedra, AO_{12}), while B remains at six (octahedral polyhedra BO_6) and the oxygen anions present a mixed coordination environment of four and two neighbors (Fig. 1). Thus, the structure of typical ABO_3 materials can be understood in terms of both cube-octahedral and octahedral clusters linked along the network and these clusters can be considered the structural motifs.

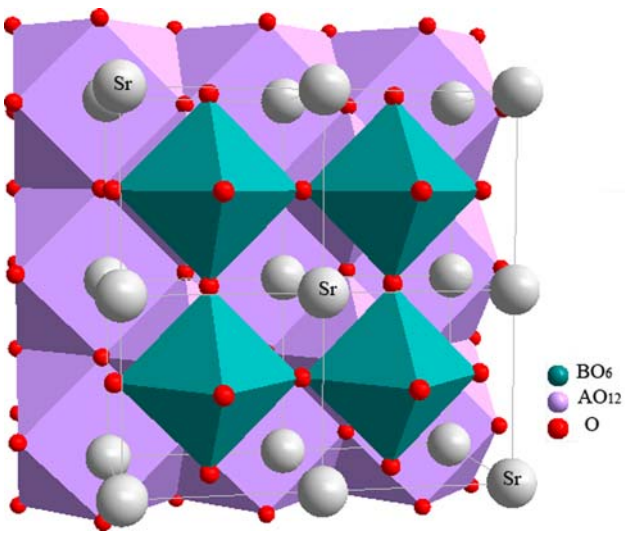

Fig. 1 Structure of typical ABO_3 perovskite with octahedral polyhedra, BO_6; and cube octahedral polyhedra, AO_{12} (color figure online)

4 Periodic models

Comparisons between simulations and experiments, while seemingly straightforward, can be easily overinterpreted or misinterpreted in terms of both the apparent quality of a simulation and the model's inability to reproduce the experimental observable of interest.

$SrTiO_3$ crystallizes in the cubic perovskite structure (space group *Pm3m*, O_h symmetry). The optimized calculated value of the *a* parameter is 3.88 Å and has been reported previously [47]. The strontium atoms share the corners of the unit cell and the titanium is at the center of the cube, surrounded by six oxygens that occupy the middle of the faces in a regular octahedral configuration. We have used a 1 × 1 × 2 supercell as a periodic model to represent the crystalline ordered ST (ST-o), which results in ten atoms in the unit cell (Fig. 2a). This ST-o can be designed as [TiO_5–O–TiO_5], since each titanium is surrounded by six O in an O_h configuration.

$SrZrO_3$ crystallizes in an orthorhombic structure. The unit cell has 20 atoms containing four units of $SrZrO_3$ as well as four nonequivalent atoms. We have used a unit cell as a periodic model to represent the crystalline ordered SZ (SZ-o) (Fig. 2c). The calculated lattice constants of the structure are $a = 5.78$ Å, $b = 5.79$ Å and $c = 8.15$ Å and the model can be designed as a [ZrO_5–O–ZrO_5] complex cluster.

Previous X-ray absorption near edge structure (XANES) experimental results [37] on the disordered phase of $SrTiO_3$ pointed to the coexistence of two types of environments for titanium, namely, fivefold titanium coordination and sixfold titanium coordination.

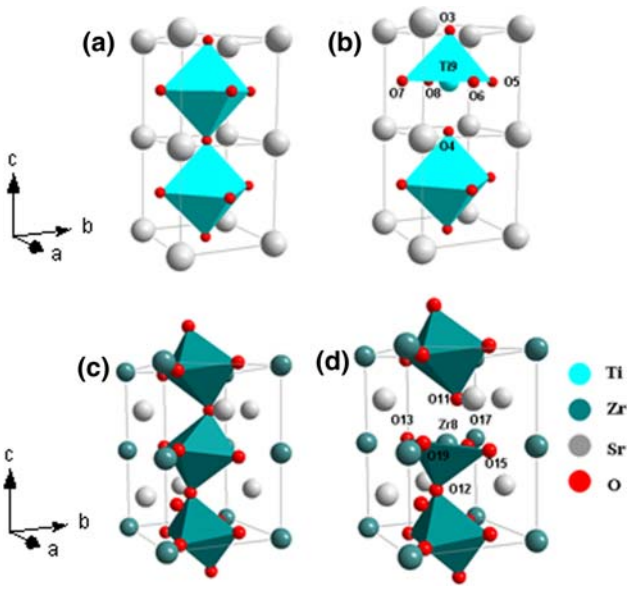

Fig. 2 **a** The ordered model of symmetric ST-o; **b** the asymmetric ST-f model of network former dislocation (Ti); **c** the ordered model of symmetric SZ-o; and **d** the asymmetric SZ-f model of network former dislocation (Zr) (color figure on-line)

Based on these experimental results, the disordered network former ST (ST-f) was modeled by shifting the titanium 9 by a (0 0 0.2) Å vector from its previous position in the 1 × 1 × 2 supercell. Using the same criteria, the zirconium 8 was shifted from its previous position in the former unit cell by a (0 0 0.2) Å vector, modeling the distorted SZ network former lattice (SZ-f). These displacements render the unit cell asymmetric, with Ti9 and Zr8 now surrounded by 5 oxygens in a square-base pyramidal configuration, while Ti10 and Zr2 are surrounded by the remaining 6 oxygens, as in the case of ST-o and SZ-o, respectively. Therefore, this asymmetric ST-f and SZ-f model represents a distortion in the network former clusters. This structure can be designated as [TiO_5–O···TiO_5] for ST-f (Fig. 2b) and as [ZrO_5–O···ZrO_5] for SZ-f (Fig. 2d).

Ab initio calculations were carried out with the CRYSTAL98 [50] package within the framework of the density-functional theory (DFT), using the gradient-corrected correlation functional proposed by Lee, Yang, and Parr, combined with the Becke3 exchange functional, B3LYP [51, 52], which was demonstrated by Muscat et al. [53] to be suitable for calculating structural parameters and band structures for a wide variety of solids. The atomic centers were described by all the electron basis sets for the SZ model: 31(3d)G for Sr, 311d31G for Zr, and 6-31G* for O [54] and for the ST model: 976-41(*d*51)G for Sr, 86-411(*d*31)G for Ti, and 6-31G* for O [54]. To simulate the displacement of the Zr and Ti atoms, we used the ATOMDISP option contained in the CRYSTAL program.

The density of states (DOS) and energy band structures were calculated with the total 0.2 Å vector dislocation of the network former in the two dislocated models.

It should be noted that our models are not meant to represent the exact reality of disordered structures but to offer a simple scheme serving to shed light on the effects of structural deformation on the network former and on the electronic structure without completely suppressing the geometry of the cell, which is useful for periodic calculations. These models can be useful for representing the quasi-crystalline material, as well as intrinsic structural defects that derive from the presence of [TiO_5–O···TiO_5] or [ZrO_5–O···ZrO_5] complex clusters.

5 Results and discussion

Figures 3a and 4a, respectively, illustrate the evolution of the XRD patterns of ST powders annealed at 400, 450 and 550 °C and of SZ powders annealed at 400, 475 and 660 °C for 2 h in oxygen flow atmosphere. XRD

diffraction peaks are visible for ST annealed at 550 °C and SZ annealed at 660 °C, indicating that, at these temperatures, both powders possess a long-range structural order. Moreover, the XRD pattern of the ST annealed at 550 °C indicates that this material possesses a single phase, allowing it to be completely indexed on the basis of the cubic structure, JCPDS card no. 35-0734 (*Pm3m*). The XRD pattern of the SZ annealed at 660 °C also indicates that this material possesses a single phase and that it can be indexed on the basis of the orthorhombic structure, JCPDS card no. 44-0161 (*Pbnm*).

The absence of a crystalline lattice requires a probabilistic description of the atomic structures of amorphous materials, giving rise to weaker and more diffuse diffracted intensity than Bragg peak intensities. Even structurally disordered (amorphous) materials are known to possess some degree of ordered, quasi-amorphous, and quasi-crystalline materials. The structure of glass, for example, presents an intermediate-range order, i.e., it has longer order over length scales than those associated with short-range order, but not as extensive as to constitute long-range order [55, 56].

Previous XANES results in the short-range order of ST [37] and SZ [38] on quasi-crystalline and quasi-amorphous samples revealed the presence of sixfold and fivefold coordinations for titanium and zirconium above 500 °C. In this context, the samples annealed at 400 °C can be considered as quasi-amorphous and more disordered structures, while those annealed at 450 °C (ST) and 475 °C (SZ) can be considered as quasi-crystalline and more ordered structures.

Figures 3b and 4b, respectively, exhibit PL spectra of ST and SZ measured at room temperature and excited at 350.7 nm.

The profile of the emission band is typical of a multiphonon and multilevel process, i.e., a system in which relaxation occurs by several paths, involving the participation of numerous states within the band gap of the material. This behavior is related to the structural disorder of ST and SZ and indicates the presence of additional electronic levels in the forbidden band gap of the material.

Qualitative measurements showed that the intensity of the SZ powders was much greater (tenfold) than that of the ST powders. The disordered (quasi-amorphous) SZ and ST powders annealed at 400 °C presented low intensity emission, while PL emission in the ordered (crystalline) powders annealed at 660 °C (SZ) and 550 °C (ST) was absent. Hence, maximum PL emission in both cases occurred in the ordered-disordered powders (quasi-crystalline) annealed at 475 °C (SZ) and at 450 °C (ST).

The strength of the electron–phonon interaction can be ascribed to the difference between the excitation and the maximum emission (Stokes shift). The SZ powder annealed at 475 °C showed maximum emission at 433 nm in the violet-blue region of the visible spectra, while the ST powder annealed at 450 °C displayed maximum emission at 550 nm in the green region of the visible spectra. This indicates the strong dependence of the electron–phonon interaction on the excitation wavelength and on the structure of the lattice. Note that the Stokes shift is smaller in the disordered SZ powder (at both 400 and 475 °C). Lattice rearrangement was clearly detected by experimental PL measurements (Stokes shift) when the annealing temperature of SZ changed from 400 to 475 °C and that of ST from 400 to 450 °C, indicating that this measurement is highly sensitive to structural changes. Raising the annealing temperature caused the structure of the powders to become more ordered, favoring violet-blue light emission by SZ and green-light emission by ST.

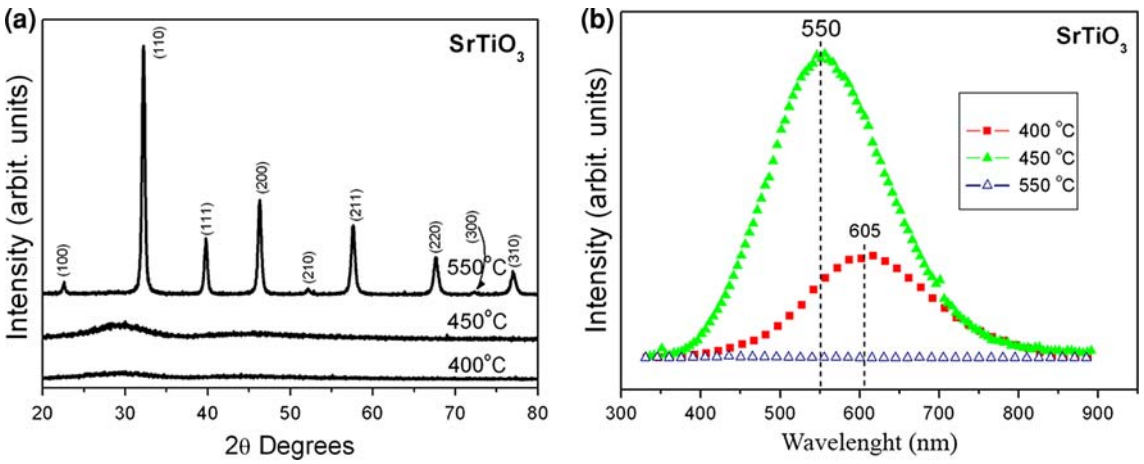

Fig. 3 **a** XRD patterns of ST; and **b** photoluminescence spectra for the ST powders annealed at 400, 450, and 550 °C for 2 h in an oxygen flow atmosphere (color figure on-line)

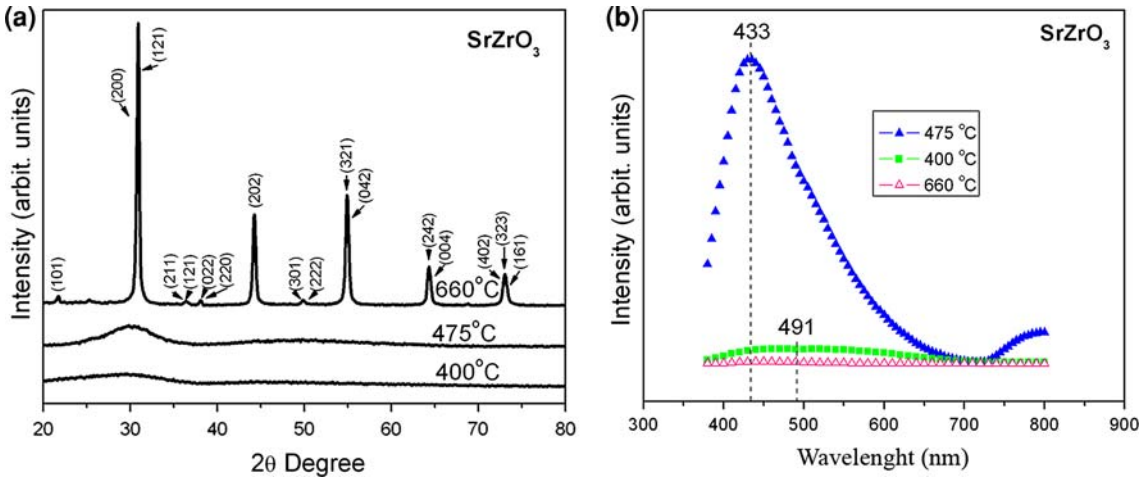

Fig. 4 **a** XRD patterns of SZ; and **b** photoluminescence spectra for the SZ powders annealed at 400, 475, and 660 °C for 2 h in an oxygen flow atmosphere (color figure on-line)

Thus, materials reveal the secrets of their structure on a length scale. These secrets are relevant in shedding light on several outstanding issues in materials science, clarifying the relationships existing between local, intermediate- and long-range structures and the properties of materials. Careful experiments, allied to theory, modeling, and simulations, will be required to pick apart the origins of these relationships. Experimental probes can provide more structural information on short- and long-range orders in materials; however, their structures over the intermediate range are still little understood. Theoretical calculations and computer simulations can complement experimental methods and have revealed new insights into medium-range order and dynamic changes in local structure.

To understand the relationship between the structural disorder in complex clusters, with an intermediate-range interaction (interaction between two clusters) and the resulting electronic defects that are generated, a detailed theoretical study was made of the electronic structure of the ordered (SZ-o and ST-o) models and of the disordered (SZ-f and ST-f) periodic models. To appreciate the differences in the electronic structure, it is opportune to make reference to quantities such as the band structures and density of states (DOS), which can be compared to each other independently of the crystalline space group.

Figure 5a shows the calculated band structure of bulk ST-o. The top of the valence band (VB) is at the M point and is very close to the X point. The bottom of the conduction band (CB) is at the Γ point. The minimal indirect gap between M and Γ is 3.69 eV and is close to the experimental one deduced from the optical absorption edge, which was found to be 3.5 eV [47].

The calculated band structure of bulk ST-f is depicted in Fig. 5b. The top of the VB is at M point and bottom of CB is at Γ, as in the case of ST-o. The indirect minimal gap between M and Γ is 3.45 eV.

For the ST-o (Fig. 5a), the valence bands are derived from O ($2p_x$, $2p_y$, $2p_z$) atomic orbitals. These orbitals are separated by an indirect gap from the first conduction band, which derives from transition-metal titanium ($3d_{xy}$, $3d_{xz}$, $3d_{yz}$) atomic orbitals, designated as "t_{2g}" by comparison with the [TiO_6] regular cluster. Above these six bands come four Ti ($3d_{x^2-y^2}$ and $3d_{z^2}$) character bands designated as "e_g". For the dislocated model (ST-f), although the VB is globally constituted of O ($2p_x$, $2p_y$, $2p_z$) character states, the top depends mainly on the axial oxygen located at the center of the structure. The CB is composed of the 3*d* states of titanium, in an apparently random splitting of bands.

The calculated total projected DOS ranges from −4 eV below the top of the VB to 8 eV above. In the case of ST-o, the upper VB is predominately composed of the O (2*p*) states distributed equally among the axial O3 and O4 oxygens and O5, O6, O7, and O8 planar oxygens of the structure (Fig. 5a). In the case of ST-f (Fig. 5b), although the VB is also composed of O (2*p*) states, the upper part, i.e., the new states, present a strong O3, O4 character, the oxygen atom that loses its connection with Ti9 (Fig. 2). The CB is clearly composed of the Ti (3*d*) states in the ordered and disordered structures. The Ti–O covalent bond makes a limited Ti (3*d*) contribution to the O (2*p*) region as well as a weak O (2*p*) contribution to the Ti (3*d*) area. The Sr (5*s*) states (not shown) are to be found in energies above −10 eV and more dispersed in the case of disordered models. These levels are weakly hybridized with oxygen levels in the ST-f model.

Figure 6a depicts the calculated band structure of bulk SZ-o. The top of the VB is very close to the S point, while the bottom of the conduction band CB is very close to the

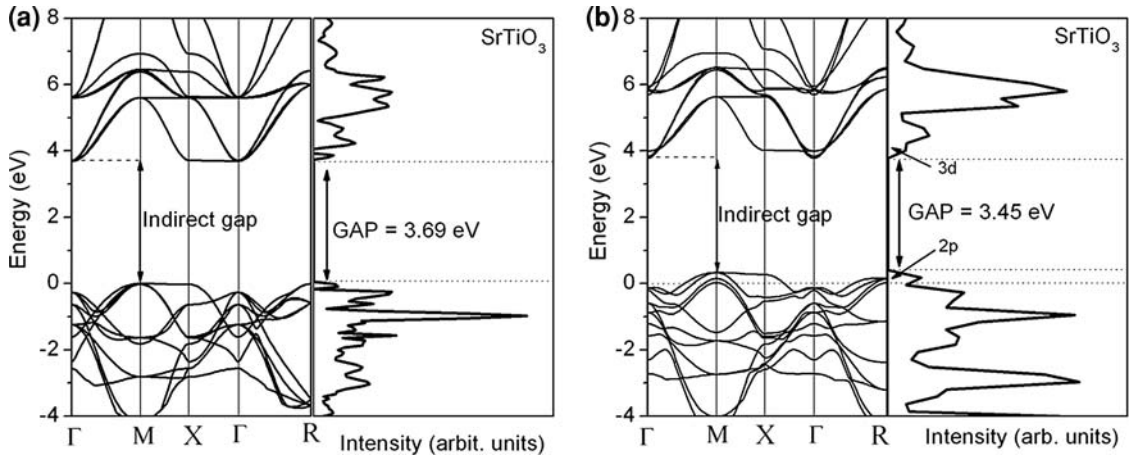

Fig. 5 Calculated total density of states and band structure for: **a** ST-o model, and ST-f model. The zero was set at the Fermi energy calculated for the ST-o model

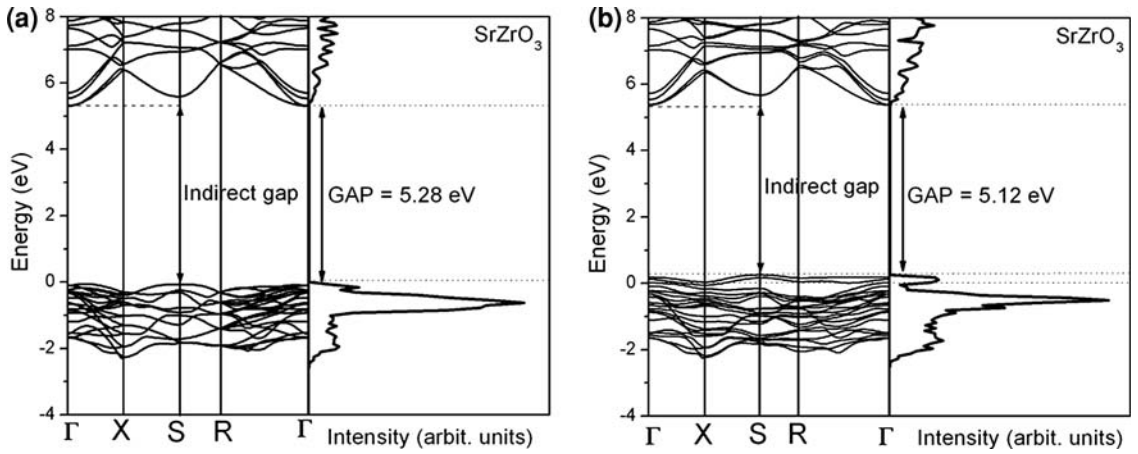

Fig. 6 Calculated total density of states and band structure for: **a** SZ-o model; and SZ-f model. The zero was set at the Fermi energy calculated for the ST-o model

Γ point. The minimal indirect gap between S and Γ is 5.28 eV and is close to the experimental one deduced from the optical absorption edge, which was reported previously to be 5.22 eV [17].

The calculated band structure of bulk SZ-f is depicted in Fig. 6b. The top of the VB is close to S point and bottom of CB is close to Γ, as in case of SZ-o. The indirect minimal gap between S and Γ is 5.12 eV.

For the SZ-o, the valence bands are derived from $2p_x$, $2p_y$, and $2p_z$ orbitals of O atoms. These bands are separated by an indirect gap from the first conduction band, which derives from transition-metal zirconium ($4d_{xy}$, $4d_{xz}$, and $4d_{yz}$) atomic orbitals, designated as "t_{2g}" by comparison with the [ZrO_6] regular cluster. Above these six bands come four Zr ($4d_{x^2-y^2}$and$4d_{z^2}$) character bands designated as "e_g". In the displaced model (SZ-f), although the VB is globally constituted of O ($2p_x$, $2p_y$, and $2p_z$) character states, the top depends mainly on the axial oxygen located at the center of the structure, O11 and O12. The CB is composed of the 4*d* states of zirconium.

Figure 6 depicts the calculated total DOS ranging from −4 eV below the top of the VB to 8 eV above. In the case of SZ-o, the upper VB is composed predominantly of the O (2*p*) states distributed equally in the O11 and O12 axial oxygens and the O13, O15, O17, and O19 planar oxygens of the structure (Fig. 6a). In the case of SZ-f (Fig. 6b), although the VB is also composed of O (2*p*) states, the upper part, i.e., the new states, present a strong axial oxygen O11, O12 character, the oxygen atom that loses its connection with Zr8 (Fig. 2). The CB is clearly composed of the Zr (4*d*) states in the ordered and disordered structures. The Zr–O covalent bond makes a limited Zr (4*d*) contribution to the O (2*p*) region as well as a weak O (2*p*) contribution to the Zr (4*d*) area, as in the case of the ST-f model.

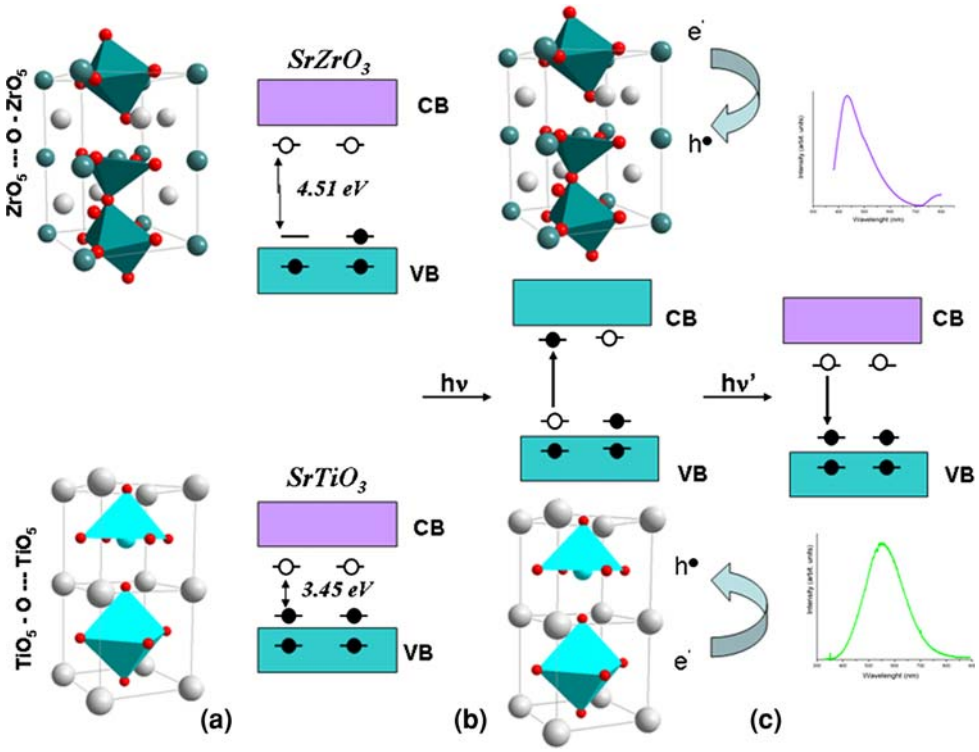

Fig. 7 Wide-band model: **a** before excitation of quasi-crystalline ZrO_5–O···ZrO_5 and TiO_5–O···TiO_5; **b** excitation—formation of STE; **c** after excitation—recombination of e^- and h^+; violet-blue luminescence of SZ and green luminescence of ST (color figures on-line)

In disordered SZ and ST powders, oxygen displacement gives rise to complex clusters. These complex clusters in titanates and zirconates can occur in three different charge states: the [TiO_5–O···TiO_5] or [ZrO_5–O···ZrO_5] complex states, which present two paired electrons ↑↓ and are neutral relative to the crystalline lattice. The second is the singly ionized [TiO_5–O···TiO_5] or [ZrO_5–O···ZrO_5] complex state, which has one unpaired electron ↑ and represents quasi-crystalline and quasi-amorphous complex clusters. The third is the [TiO_5–O···TiO_5] or [ZrO_5–O···ZrO_5] complex state, which does not trap any electrons—and is doubly positively charged with respect to the lattice and can be linked to the amorphous state. Another portion of electrons and holes may be trapped by intrinsic crystal defects in the network modifier complex clusters.

These titanium, zirconium, and strontium complexes induce new energy states in the band gap, as reported previously in the discussion on the electronic band structure and total density of states. These can be attributed to the titanium–oxygen, zirconium–oxygen, and strontium–oxygen complex clusters. Geometrical alterations in these clusters, such as distortions, breathing, and tilt, create an innumerable variety of structures and hence distinct material properties.

Quantum-mechanical calculations of dislocated [TiO_5–O···TiO_5] or [ZrO_5–O···TiO_5] complex clusters indicate that localized states generated in the band gap reduce the gap energies. When the structural order increases, the gap energy increases. These findings confirm the fact that PL is directly associated with the localized states existing in the band gap. Distorted clusters cause local lattice distortion that propagates throughout the material, pushing the surrounding clusters away from their ideal positions. Thus, distorted clusters must move for these properties to occur, changing the electronic distribution along the network of these polar clusters. This electronic structure dictates both optical and electrical transport properties and plays a major role in determining reactivity and stability. However, these movements can be induced within the crystal lattice by PL measurements and these anisotropic cooperative movements lead to these properties.

The band gap of ST is comparatively smaller than that of SZ. Therefore, the excitation wavelength of 350.7 nm is able to excite different populations of electrons in the band gap of the two structures. Here, each color represents a different type of electronic transition and is linked to a specific structural arrangement. In the case of ST, the recombination of electrons and holes gives rise to green-light emission and in that of SZ to very intense violet-blue light emission.

In our model, the wide-band model [57] shown in Fig. 7, the most important events occur before excitation, i.e., before the photon arrives. The deep and shallow defects generated by the complex clusters give rise to localized states in the band gap and inhomogeneous charge distribution in the cell, allowing electrons to become trapped (Fig. 7). The localized levels are energetically distributed so that various energies are able to excite the trapped electrons.

In these complexes, the $[BO_5–O]^{\cdot}$ species acts as an electron donor, while the complexes $[BO_5\cdots O]^{\cdot}$ tend to trap electrons and/or holes and the complexes $[BO_5\cdots O\cdots BO_5]^{\cdot\cdot}$ act as electron traps. After excitation of the photon, the process of recombination and decay follows the several valid hypotheses proposed in the literature [27–36].

In this paper we have shown that distinct structures and different orders–disorders in the lattice produce different types of PL emission. The complex clusters already existing in the ground state facilitate the emission process and lead to PL, i.e., radiative recombination. Thus, the distortions of complex clusters are crucial for an understanding of the properties of materials.

6 Conclusions

In summary, ultrafine crystalline, quasi-crystalline, and quasi-amorphous $SrZrO_3$ and $SrTiO_3$ powders were synthesized by soft chemical processing. PL measurements indicated an intense violet-blue light in SZ and a less intense green light emission in ST quasi-crystalline powders. As the order of the lattice increased, the PL emission in both powders disappeared. The PL results can be attributed to the distortions in the materials' polyhedral constituents (octahedral and dodecahedral clusters). The different electronic levels appearing in the band gap of ST and SZ powders are able to create different color emissions in the visible spectra of light. This effect was confirmed by first-principles calculations based on the B3LYP density functional theory using disorder models of the lattice.

The map shown here offers a conceptual framework to understand, discuss, and optimize electronic material properties on the basis of their constituent polyhedra. The interactions of the clusters in the solid provide important information about molecular movements and reactivity towards external stimuli, and this information was used successfully to induce complete PL emission. However, the mechanistic pathway of PL emission is still not completely understood. Understanding it may provide information about how clustered molecules "communicate" with one another in physical and chemical processes.

Acknowledgments The authors thank the Brazilian research funding institutions FAPESP/CEPID, CNPq/PRONEX and CAPES for backing this work. J.A. acknowledges the Ministerio de Educación y Cultura of the Spanish Government for financing his research stay.

References

1. Lines ME, Glas AM (1977) Principles and applications of ferroelectrics and related materials. Claredum, Oxford
2. Hsiang HI, Hsi CS, Huang CC, Fu SL (2008) Sintering behavior and dielectric properties of $BaTiO_3$ ceramics with glass addition for internal capacitor of LTCC. J Alloy Compd 459:307
3. Bannikov VV, Shein IR, Kozhevnikov VL, Ivanovskii AL (2008) Magnetism without magnetic ions in non-magnetic perovskites $SrTiO_3$, $SrZrO_3$ and $SrSnO_3$. J Magn Magn Mater 320:936
4. Takahashi Y, Konishi T, Soga K, Funwara T (2008) Origin of photoluminescence in suzukiite-type $BaTiSi_2O_7$. J Ceram Soc Jpn 116:1104
5. Luo L, Ren HZ, Tang XG, Ding CR, Wang HZ, Chen XM, Jia JK, Hu ZF (2008) Room temperature tunable blue-green luminescence in nanocrystalline (Pb1-*x*Sr*x*)TiO_3 thin film grown on yttrium-doped zirconia substrate. J Appl Phys 104:043514
6. Liu AY, Xue JQ, Meng XJ, Sun JL, Huang ZM, Chu JH (2008) Infrared optical properties of Ba(Zr0.20Ti0.80)O-3 and Ba(Zr0.30Ti0.70)O-3 thin films prepared by sol-gel method. Appl Surf Sci 254:5660
7. Sambrano JR, Longo VM, Longo E, Taft CA (2007) Electronic and structural properties of the (001) $SrZrO_3$ surface. Theochem J Mol Struct 813:49
8. Iwahara H, Yajima T, Hibino T, Ushida H (1993) Performance of solid oxide fuel-cell using proton and oxide-ion mixed conductors based on bace1-Xsmxo3-Alpha. J Electrochem Soc 140:1687
9. Kurita N, Fukatsu N, Ohashi T (1994) Hydrogen analyzer based on coulometric titration using proton conduction solid-electrolyte. J Jpn Inst Met 58:782
10. Yajima T, Koide K, Takai H, Fukatsu N, Iwahara H (1995) Application of hydrogen sensor using proton conductive ceramics as a solid-electrolyte to aluminum casting industries. Solid State Ion 79:333
11. Mimuro S, Shibako S, Oyama Y, Kobayashi K, Higuchi T, Shin S, Yamaguchi S (2007) Proton incorporation and defect chemistry of Yb-doped $BaPrO_3$. Solid State Ion 178:641
12. Roth RS (1957) Classification of perovskite and other Abo3-type compounds. J Res Natl Bur Stand 58:75
13. Swanson HE, Tatge E (1951) Standard X-ray diffraction patterns. Acta Crystallogr Sect B-Struct Sci 46:318
14. deLigny D, Richet P (1996) High-temperature heat capacity and thermal expansion of $SrTiO_3$ and $SrZrO_3$ perovskites. Phys Rev B 53:3013
15. Kennedy BJ, Howard CJ, Chakoumakos BC (1999) High-temperature phase transitions in $SrZrO_3$. Phys Rev B 59:4023
16. Matsuda T, Yamanaka S, Kurosaki K, Kobayashi S (2003) High temperature phase transitions of $SrZrO_3$. J Alloy Compd 351:43
17. Cavalcante LS, Simoes AZ, Sczancoski JC, Longo VM, Erlo R, Escote MT, Longo E, Varela JA (2007) $SrZrO_3$ powders obtained by chemical method: synthesis, characterization and optical absorption behaviour. Solid State Sci 9:1020
18. Chen CH, Zhu WG, Chen XF, Yu T, Yao X (2003) Preparation and characteristic study of MOD derived dielectric $SrZrO_3$ thin films. Ferroelectrics 292:29
19. Capizzi M, Frova A (1970) Optical gap of strontium titanate (deviation from Urbach tail behavior). Phys Rev Lett 25:1298
20. Hasegawa T, Shirai M, Tanaka K (2000) Localizing nature of photo-excited states in $SrTiO_3$. J Lumines 87–9:1217
21. Suzuki H, Bando H, Ootuka Y, Inoue IH, Yamamoto T, Takahashi K, Nishihara Y (1996) Superconductivity in single-crystalline $Sr_{1-x}La_xTiO_3$. J Phys Soc Jpn 65:1529
22. Koonce CS, Cohen ML, Schooley JF, Hosler WR, Pfeiffer ER (1967) Superconducting transition temperatures of semiconducting Srtio3. Phys Rev 163:380
23. Zhang WF, Tang JW, Ye JH (2006) Photoluminescence and photocatalytic properties of $SrSnO_3$ perovskite. Chem Phys Lett 418:174

24. Chapman BD, Stern EA, Han SW, Cross JO, Seidler GT, Gavrilyatchenko V, Vedrinskii RV, Kraizman VL (2005) Diffuse X-ray scattering in perovskite ferroelectrics. Phys Rev B 71:020102
25. Zhang MS, Yu J, Chu JH, Chen Q, Chen WC (2003) Microstructures and photoluminescence of barium titanate nanocrystals synthesized by the hydrothermal process. J Mater Process Technol 137:78
26. Longo E, Orhan E, Pontes FM, Pinheiro CD, Leite ER, Varela JA, Pizani PS, Boschi TM, Lanciotti F, Beltran A, Andres J (2004) Density functional theory calculation of the electronic structure of Ba0.5Sr0.5TiO3: photoluminescent properties and structural disorder. Phys Rev B 69:125115
27. Landau LD (1933) Phys Z Sowjetunion 3:644
28. Qiu Y, Jiang YJ, Tong GP, Zhang JF (2008) Dynamic process of self-trapped polaron in photoexcited $SrTiO_3$. Phys Lett A 372:2920
29. Leonelli R, Brebner JL (1986) Time-resolved spectroscopy of the visible emission band in strontium–titanate. Phys Rev B 33:8649
30. Eglitis RI, Kotomin EA, Trepakov VA, Kapphan SE, Borstel G (2002) Quantum chemical modelling of electron polarons and 'green' luminescence in $PbTiO_3$ perovskite crystals. J Phys Condes Matter 14:L647
31. Meng JF, Huang YB, Zhang WF, Du ZL, Zhu ZQ, Zou GT (1995) Photoluminescence in Nanocrystalline Batio3 and Srtio3. Phys Lett A 205:72
32. Vikhnin VS, Kaplyanskii AA, Kutsenko AB, Liu GK, Beitz JV, Kapphan SE (2001) "Charge transfer-lattice" clusters induced by charged impurities. J Lumines 94:775
33. Vikhnin VS, Eglitis RI, Kapphan SE, Kotomin EA, Borstel G (2001) A new phase in ferroelectric oxides: the phase of charge transfer vibronic excitons. Europhys Lett 56:702
34. Vikhnin VS, Kapphan S (1998) Vibronic charge-transfer excitons: possible nature of the unusual properties of virtual perovskitelike ferroelectrics. Phys Sol Stat 40:834
35. Eglitis RI, Kotomin EA, Borstel G, Kapphan SE, Vikhnin VS (2003) Semi-empirical calculations of the electronic and atomic structure of polarons and excitons in ABO(3) perovskite crystals. Comput Mater Sci 27:81
36. Meng JF, Rai BK, Katiyar RS, Zou GT (1997) Study of visible emission and phase transition in nanocrystalline $A_{(1-x)}A'_xTiO_3$ systems. Phys Lett A 229:254
37. Longo VM, de Figueiredo AT, de Lazaro S, Gurgel MF, Costa MGS, Paiva-Santos CO, Varela JA, Longo E, Mastelaro VR, De Vicente FS, Hernandes AC, Franco RWA (2008) Structural conditions that leads to photoluminescence emission in $SrTiO_3$: an experimental and theoretical approach. J Appl Phys 104:023515
38. Longo VM, Cavalcante LS, Erlo R, Mastelaro VR, de Figueiredo AT, Sambrano JR, de Lazaro S, Freitas AZ, Gomes L, Vieira ND, Varela JA, Longo E (2008) Strong violet-blue light photoluminescence emission at room temperature in $SrZrO_3$: joint experimental and theoretical study. Acta Mater 56:2191
39. Schroder DK (1990) Semiconductor material and device characterization. Wiley, New York
40. Cuong DD, Lee B, Choi KM, Ahn HS, Han S, Lee J (2007) Oxygen vacancy clustering and electron localization in oxygen-deficient $SrTiO_3$: LDA + U study. Phys Rev Lett 98:115503
41. Onishi T (2008) The Hybrid-DFT study on bandgap estimation for the perovskite-type titanium oxide of $SrTiO_3$. Int J Quantum Chem 108:2856
42. Kan DS, Terashima T, Kanda R, Masuno A, Tanaka K, Chu SC, Kan H, Ishizumi A, Kanemitsu Y, Shimakawa Y, Takano M (2005) Blue-light emission at room temperature from Ar+-irradiated $SrTiO_3$. Nat Mater 4:816
43. Kan D, Kanda R, Kanemitsu Y, Shimakawa Y, Takano M, Terashima T, Ishizumi A (2006) Blue luminescence from electron-doped $SrTiO_3$. Appl Phys Lett 88:191916
44. Kan D, Sakata O, Kimura S, Takano M, Shimakawa Y (2007) Structural characterization of Ar+-irradiated $SrTiO_3$ showing room-temperature blue luminescence. Jpn J Appl Phys Part 2 Lett Express Lett 46:L471
45. Zhang CM, Li CX, Yang J, Cheng ZY, Hou ZY, Fan Y, Lin J (2009) Tunable luminescence in monodisperse zirconia spheres. Langmuir 25:7078
46. Pontes FM, Longo E, Leite ER, Lee EJH, Varela JA, Pizani PS, Campos CEM, Lanciotti F, Mastelaro V, Pinheiro CD (2003) Photoluminescence at room temperature in amorphous $SrTiO_3$ thin films obtained by chemical solution deposition. Mater Chem Phys 77:598
47. Orhan E, Pontes FM, Pinheiro CD, Boschi TM, Leite ER, Pizani PS, Beltran A, Andres J, Varela JA, Longo E (2004) Origin of photo luminescence in $SrTiO_3$: a combined experimental and theoretical study. J Solid State Chem 177:3879
48. Zhang CM, Lin CK, Li CX, Quan ZW, Liu XM, Lin J (2008) Enhanced luminescence of BPO_4 by mixing with SiO_2 and Al_2O_3. J Phys Chem C 112:2183
49. Lin CK, Luo Y, You H, Quan Z, Zhang J, Fang J, Lin J (2006) Sol-gel-derived BPO_4/Ba^{2+} as a new efficient and environmentally-friendly bluish-white luminescent material. Chem Mat 18:458
50. Saunders V, Dovesi R, Roetti C, Orlando R, Zicovich-Wilson CM, Harrison NM, Doll K, Civalleri B, Bush B, DArco PLM (2003) CRYSTAL 03 users manual. University of Torino, Torino
51. Lee CT, Yang WT, Parr RG (1988) Development of the Colle-Salvetti correlation-energy formula into a functional of the electron-density. Phys Rev B 37:785
52. Becke AD (1993) Density-functional thermochemistry. 3. The role of exact exchange. J Chem Phys 98:5648
53. Muscat J, Wander A, Harrison NM (2001) On the prediction of band gaps from hybrid functional theory. Chem Phys Lett 342:397
54. Arevalo-Lopez AM, Alario-Franco AM (2007) J Solid State Chem 180:3271
55. Salmon PS (2002) Amorphous materials—order within disorder. Nat Mater 1:87
56. Hufnagel TC (2004) Amorphous materials—finding order in disorder. Nat Mater 3:666
57. Moreira ML, Andres J, Longo VM, Li MS, Varela JA, Longo E (2009) Photoluminescent behavior of $SrZrO_3/SrTiO_3$ multilayer thin films. Chem Phys Lett 473:293